phys. stat. sol. (b) **236**, No. 2, 253–264 (2003) / **DOI** 10.1002/pssb200301664

# Modelling of defects and surfaces in perovskite ferroelectrics

**G. Borstel**[*, 1], **R. I. Eglitis**[1], **E. A. Kotomin**[2, 3], and **E. Heifets**[4]

[1] Fachbereich Physik, Universität Osnabrück, 49069 Osnabrück, Germany
[2] Max-Planck-Institut für Festkörperforschung, 70569 Stuttgart, Germany
[3] Institute of Solid State Physics, University of Latvia, Riga, Latvia
[4] California Institute of Technology, MS 139-74, Pasadena, CA 91125, USA

Received 1 July 2002, accepted 15 October 2002
Published online 7 March 2003

**PACS** 68.35.Bs, 68.47.Gh, 71.15.Ap, 73.20.At, 77.84.Dy

The results of electronic structure calculations for different terminations of $SrTiO_3$ (100) and (110) perovskite thin films are discussed. These calculations are based on the *ab initio* Hartree-Fock (HF) method and Density Functional Theory (DFT). Results are compared with previous *ab initio* plane-wave LDA and classical Shell Model (SM) calculations. Calculated considerable increase of the Ti–O chemical bond covalency nearby the surface is confirmed by experimental data. Our quantum chemical calculations performed by means of the intermediate neglect of differential overlap (INDO) method confirm the existence of self-trapped electrons in $KNbO_3$, $KTaO_3$ and $BaTiO_3$ crystals. The relevant lattice relaxation energies are 0.21 eV, 0.27 eV and 0.24 eV, and the optical absorption energies 0.78 eV, 0.75 eV and 0.69 eV, respectively. We suggest a theoretical interpretation of the so-called *green* luminescence (2.2–2.3 eV) in $ABO_3$ perovskite crystals as a result of the recombination of electrons and holes forming the Charge-Transfer-Vibronic-Exciton (CTVE). The calculated luminescence energies for $SrTiO_3$, $BaTiO_3$, $KNbO_3$ and $KTaO_3$ perovskite crystals are in a good agreement with the experimentally observed energies.

**1. Introduction** Thin films of $ABO_3$ perovskite ferroelectrics (e.g., $SrTiO_3$) are important for many technological applications, where the surface structure is important [1–4]. The $SrTiO_3$(100) surface relaxation has been experimentally studied by means of several techniques, e.g. low energy electron diffraction (LEED), reflection high-energy electron diffraction (RHEED), medium energy ion scattering (MEIS) and surface X-ray diffraction (SXRD) measurements [5–9]. Several *ab initio* [10–17] and shell model (SM) [18, 19] theoretical studies were dedicated to the (100) surface of $BaTiO_3$ and $SrTiO_3$ crystals. In order to study the dependence of the surface relaxation properties on exchange-correlation functionals and localized/plane wave basis sets used in most of calculations, recently [20] we performed a detailed comparative study of $SrTiO_3$ surface relaxation based on a number of different techniques. In this paper we analyze the relevant electronic structure of the (001) surface with emphasis on the electronic charge redistribution and gap modification, and present preliminary results for the atomic structure of the (110) surface.

The properties of $ABO_3$ ferroelectric perovskites are influenced by point defects, primarily vacancies. For instance, laser second harmonic generation in $KNbO_3$ is reduced by the blue-light-induced absorption (BLIIRA) [21]. Despite the fact that such light-induced absorption is well known for many perovskites, the effect was studied only in a few papers. Relatively little is known about intrinsic point defects in $ABO_3$. A broad absorption band around 2.7 eV has been observed in electron-irradiated

[*] Corresponding author: e-mail: gborstel@uos.de, Fax: +49-541-9692351, Phone: +49-541-9692676

 0370-1972/03/23603-0253 $ 17.50+.50/0

$KNbO_3$ crystals and ascribed tentatively to *F*-type centers (O vacancy with one or two trapped electrons) [22, 23]. Transient optical absorption around 1.2 eV has been associated recently [23], in analogy with other perovskites, with a hole polaron (a hole bound to some defect), whereas IR absorption (around 0.8 eV) with electron polarons [24]. Recently [25, 26] we performed semi-empirical calculations for the *F* centers and hole polarons bound to a K vacancy in $KNbO_3$. Based on these calculations, we confirmed the preliminary interpretation of the above-mentioned absorption bands at 1.2 eV and 2.7 eV.

Many $ABO_3$ perovskites reveal photoluminescence in the visible range. This, so-called "green" luminescence band peaks around 2.5 eV in $BaTiO_3$ [27] and at 2.2–2.3 eV in $KTaO_3$ and $KNbO_3$ [28]. The origin of this luminescence has been discussed more than once. Suggested mechanisms include donor-acceptor recombination [29], recombination of electron and hole polarons, charge-transfer vibronic excitons (CTVE) [30–32] and transitions in $MeO_6$ complexes [33]. In this paper, we perform a modelling of electron polarons and triplet excitons in $ABO_3$ perovskites and compare calculated optical energies with relevant experiments.

## 2. Computational method

**2.1 Ab initio HF and DFT method** In this study we restrict ourselves to simulations of $SrTiO_3$ in the cubic perovskite phase (stable above 105 K), with (001) surfaces terminated by a plane containing SrO or $TiO_2$ units. To simulate both surfaces, we used symmetrical slabs consisting of seven alternating $TiO_2$ and SrO layers. We simulated also the O-terminated (110) surface where surface relaxation was recently calculated by means of the SM [19].

The total energies and electronic structures of these slabs were calculated by several quite different methods: HF with different DFT-type *a posteriori* electron correlation corrections to the total energy [34] such as Generalized Gradient Approximation (HFGGA), Perdew-91 (HFPer91), Lee–Yang–Parr (HFLYP); and full-scale DFT calculations based on the Kohn–Sham equation with a number of exchange-correlation functionals, including Local Density Approximation (LDA), Generalized Gradient Approximation (GGA) by Perdew and Wang (PW), Perdew, Burke and Ernzernhof (PBE), as well as Becke exchange functionals using Beckes three-parameter method, combined with the non-local correlation functionals by Perdew and Wang (B3PW), as those by Lee, Yang, and Parr (B3LYP). For all calculations we used the CRYSTAL-98 computer code [35], in which both (HF/DFT) types of calculations are implemented on equal grounds. Unlike previous plane-wave calculations, this code uses a localized Gaussian-type basis set. In our simulations we applied the standard basis set recommended for $SrTiO_3$ [35]. Another advantage of the CRYSTAL-98 code is its treatment of purely 2D slabs, without an artificial periodicity in the direction perpendicular to the surface, commonly employed in all previous surface-band structure calculations (e.g., [10, 16]). For optimization of atomic coordinates through minimization of the total energy per unit cell, we use our own computer code that implements the Conjugated Gradients optimization technique with numerical computation of derivatives. An analysis of the optimized atomic structure for the (001) surface and comparison with above-mentioned experimental data was presented in Ref. [36].

We would like only to note here that we have tested how different methods reproduce the experimentally observable bulk properties – lattice constant $a_0$ and the bulk modulus *B*. The LDA calculations underestimate $a_0$ by 0.8% and overestimate *B* by 20%. The HF method without any correlation correc-

**Table 1** Static (Mulliken) charges of atoms calculated for the bulk $SrTiO_3$ by means of variety of DFT and HF methods.

| atom (A) | LDA | B3LYP | B3PW | BLYP | PBE | PWGGA | HF |
|---|---|---|---|---|---|---|---|
| $Sr^{2+}$ | 1.830 | 1.852 | 1.852 | 1.835 | 1.832 | 1.834 | 1.909 |
| $Ti^{4+}$ | 2.126 | 2.325 | 2.272 | 2.266 | 2.206 | 2.212 | 2.584 |
| $O^{2-}$ | −1.319 | −1.392 | −1.375 | −1.367 | −1.346 | −1.349 | −1.497 |

**Table 2** Bond populations (in milli *e*) for the bulk $SrTiO_3$. Negative populations mean atomic repulsion. I and II is the first and second nearst neighboring atoms for the bulk oxygen O(I).

| atom (A) | atom(B) | LDA | B3LYP | B3PW | BLYP | PBE | PWGGA | HF |
|---|---|---|---|---|---|---|---|---|
| O(I) | O(I) | −48 | −36 | −36 | −30 | −32 | −34 | −40 |
| | Sr(I) | −10 | −8 | −10 | −4 | −6 | −6 | −10 |
| | Ti(I) | 52 | 74 | 82 | 66 | 74 | 70 | 112 |
| | O(II) | −2 | −4 | −4 | −2 | −2 | −2 | −8 |

tions to the total energy overestimates both $a_0$ (by 1%) and $B$ (by 16%). HF with GGA corrections makes $a_0$ too small (by −1.5%), but $B$ even larger (by 41%). Lastly, the hybrid B3PW method gives a much better result for $B$ (by 4%) and overestimates $a_0$ by only 1%. In other words, the hybrid B3PW method gives the best agreement with experimental data. Table 1 presents results for the effective atomic charges. The effective charges for Ti and O ions, both in the bulk and on the surface, are much smaller than the formal ionic charges ($4e$, $-2e$, resp.). This arises due to the partly covalent nature of the Ti−O chemical bond. In contrast, the Sr charge remains close to the formal charge $+2e$. Note that these results are very close for all methods used. The Ti-O chemical bond covalency is confirmed by the bond populations in Table 2, which vary from 0.05 to 0.11$e$, dependent on the particular method. Obviously, there is no covalent bonding between any other types of atoms, e.g. Sr−O or O−O.

**2.2 INDO method** *Ab initio* methods are still time-consuming for the treatment of the electronic and atomic structure of complex systems, especially those with partly covalent chemical bonding, like perovskites. For a study of relatively complicated cases of perovskite solid solutions, defects and excitons, there is a need to close the gap between accurate but time consuming *ab initio* methods [37−40] and widely used, simple but not so accurate semi-empirical quantum chemical methods with transferable parameters valid for a wide class of systems. An example of such a method is the Intermediate Neglect of Differential Overlap (INDO) [41−43] method, which is a simplified version of the Hartree−Fock formalism.

In the last decade the INDO method has been successfully used in studies of bulk solids and defects in oxides [44−50] and semiconductors [51]. This method has been applied earlier to the study of phase transitions and frozen phonons in pure $KNbO_3$ [52], pure and Li doped $KTaO_3$ [53], solid perovskite solutions $KNb_xTa_{1-x}O_3$ [54, 55], as well as $F$ centers and hole polarons in $KNbO_3$ [56−58].

The detailed analysis of the development of the INDO parametrization for pure $KNbO_3$ and $KTaO_3$ is given in Refs. [52, 53] whereas for $BaTiO_3$ and $SrTiO_3$ in Refs. [59, 60]. The INDO method reproduces very well both available experimental data and results of *ab initio* LDA-type calculations. In particular, this method reproduces the effect of ferroelectric instability of $KNbO_3$ due to off-centre displacement of Nb atoms from the regular lattice sites, as well as the relative magnitudes of the relevant energy gains for the [100], [110], [111] Nb displacements. These are consistent with the sequence of the stability of the tetragonal, orthorhombic and rhombohedral phases, respectively, as the crystals temperature decreases. This is a very non-trivial achievement, since the typical energy gain due to the Nb off-centre displacement is only of the order of several mRy per unit cell. In these calculations we use supercells of 135 atoms.

**3. Ab initio modeling of the (001) surface** Since our atomic displacements in the outermost $SrO/TiO_2$ planes were analyzed recently [20, 36], we want only to stress here that our Gaussian-basis results are in qualitative agreement with previous plane-wave calculations [10, 16]. Both DFT and HF with incorporation of correlation effects predict larger Sr displacement on the SrO-terminated surface than that for Ti atoms on the $TiO_2$-terminated surface, also in agreement with previous *ab initio* calculations. For the $TiO_2$ termination *all* theoretical methods predict the surface O atom to relax inwards, in contrast to the SrO termination. Relaxation of atoms in the third plane is already quite small. In all calculations the surface energy for SrO termination is slightly smaller than for the $TiO_2$ termination. However, the energy

**Table 3** Charge densities in the (001) crystalline planes of the bulk $SrTiO_3$ (in *e*, per $TiO_2$ or SrO unit).

| unit | LDA | B3LYP | B3PW | BLYP | PBE | PWGGA | HF |
|---|---|---|---|---|---|---|---|
| $TiO_2$ | −0.512 | −0.459 | −0.478 | −0.468 | −0.486 | −0.486 | −0.410 |
| SrO | 0.511 | 0.46 | 0.477 | 0.468 | 0.486 | 0.485 | 0.412 |

difference is small and thus *both* surfaces are energetically nearly equally favourable, in agreement with the experimental observation [5]. Note that the surface energy of 1.37 eV per cell, which was calculated for a $TiO_2$-terminated surface by the shell model [19], is also slightly larger than the surface energy for SrO-termination (1.33 eV/cell). The *ab initio* LAPW calculations [14] gave similar average surface energies of 1.27 eV per cell.

A comparison of a series of our HF and DFT calculations for the surface rumpling and interatomic distance changes with the two previous *ab initio* plane-wave studies [10, 16] and classical SM calculations [19] shows good agreement for all functionals used [36]. All theoretical methods (both quantum mechanical, irrespective on particular exchange-correlation functionals and basis set type, and classical SM) give the same signs for both the rumpling and the change of the interplanar distances. They predict much larger rumpling for the SrO surface in comparison to that for the $TiO_2$ surface, compression of the distance between the first and second planes, and its expansion for the second and third planes.

For all methods used the cation charges in two top layers in the SrO-terminated surface turn out to be smaller than in the bulk. In contrast, the O negative charges in these layers become even more negative, due to additional electron charge transfer. Changes in atomic charges in deeper layers become very small, their sign vary, dependent on the exchange-correlation functional used. These effects are more strongly pronounced in the case of a $TiO_2$-terminated surface. In particular, charge reduction of surface Ti ions (−0.132*e*) is much larger than that on the SrO-terminated surface (−0.027*e*). Charges of Sr ions in the subsurface layer of $TiO_2$-terminated surface are close to Sr charges in the top layer of SrO-terminated surface. In the third layer Ti charges are still reduced, but the magnitude of the charge reduction is relatively small. Sr charges in the central layer of the slab are essentially the same as in the $SrTiO_3$ bulk. In contrast, the O charges are reduced through the entire $TiO_2$-terminated slab. This O charge reduction is especially large in the top two layers nearby the surface.

Tables 3, 4 and 5 give the difference in the charge densities at [001] planes in the $SrTiO_3$ bulk and on the (001) surfaces for both terminations, respectively. As one can see, the additional charge is mostly localized on the $TiO_2$ unit in the first or second plane, dependent on the termination. This is true for all exchange-correlation functionals used for $TiO_2$ termination, and for most functionals for the SrO termination (except for BLYP and HF). In the latter case the additional charge located at the top SrO layer just a little bit exceeds the additional charge at the subsurface $TiO_2$ layer. The above-described charge redistribution is in a line with ideas of *a weak polarity* [2]. Ion polarization at surfaces with both terminations is significant in the top two planes and becomes very small in deeper layers.

On the SrO-terminated surface both Sr and O ions have negative dipole moments. This means that their dipole moments are directed inwards to the surface (direction outwards from the surface is chosen

**Table 4** Changes in the charge density with respect to the bulk in four top planes (I to IV) of the $TiO_2$-terminated (001) slab.

| unit | LDA | B3LYP | B3PW | BLYP | PBE | PWGGA | HF |
|---|---|---|---|---|---|---|---|
| $TiO_2$(I) | 0.172 | 0.142 | 0.161 | 0.136 | 0.156 | 0.161 | 0.127 |
| SrO(II) | 0.065 | 0.067 | 0.059 | 0.072 | 0.056 | 0.066 | 0.060 |
| $TiO_2$(III) | 0.019 | 0.020 | 0.021 | 0.025 | 0.030 | 0.019 | 0.011 |
| SrO(IV) | 0.002 | 0.001 | 0.000 | 0.001 | 0.000 | 0.001 | 0.008 |

**Table 5** Same as Table 4 for the SrO-terminated (001) slab.

| Unit | LDA | B3LYP | B3PW | BLYP | PBE | PWGGA | HF |
|---|---|---|---|---|---|---|---|
| SrO(I) | −0.061 | −0.086 | −0.088 | −0.112 | −0.101 | −0.101 | −0.096 |
| $TiO_2$(II) | −0.201 | −0.127 | −0.128 | −0.101 | −0.127 | −0.127 | −0.088 |
| SrO(III) | 0.006 | −0.014 | −0.018 | −0.015 | −0.012 | −0.008 | −0.013 |
| $TiO_2$(IV) | 0.006 | −0.011 | −0.007 | −0.014 | −0.008 | −0.009 | −0.013 |

as positive). The dipole moments of Sr ions are surprisingly large, only by ≈30% less then those for surface oxygen ions. In the subsurface layer of the SrO terminated surface Ti atoms also reveal considerable negative dipole moments. These moments are smaller by ≈60% than those of the surface cations. Polarization of Sr ions in the third layer is very small, but still found negative for all used functionals. Polarization of O ions in the subsurface layer, as well as in the next third layer, is also insignificant. For most functionals used the O dipole moments in these layers are negative. The only exception are calculations with LDA and B3LYP functionals giving the positive dipole moments for the subsurface O ions, and LDA calculations for O ions in the third layer. However, these effects are very delicate since dipole moments are very small.

On the $TiO_2$-terminated surface the polarization of cations has an opposite sign compared to the SrO-terminated surface, surface Ti ions now reveal positive dipole moments. The polarization value is approximately the same, but with an opposite sign as compared with subsurface Ti for the SrO-termination. Dipole moments on the subsurface Sr ions are small but still positive. In the third layer the dipole moments on Ti ions turn out to become negative (for all methods except HF). Oxygen polarization on the $TiO_2$-terminated surface is surprisingly small. In the surface layer calculated O dipole moments are negative for most functionals, except for PBE and PWGGA. These moments become positive on the subsurface O ions and, again, negative on the O ions in the third layer.

**Table 6** The bond populations (in milli *e*) for $TiO_2$ termination. I to IV are numbers of planes enumerated from the surface.

| atom(A) | atom(B) | LDA | B3LYP | B3PW | BLYP | PBE | PWGGA | HF |
|---|---|---|---|---|---|---|---|---|
| O(I) | O(I) | −36 | −28 | −30 | −24 | −26 | −26 | −34 |
| | Ti(I) | 108 | 124 | 128 | 114 | 118 | 114 | 146 |
| | Sr(II) | −10 | −10 | −10 | −4 | −4 | −6 | −28 |
| | O(II) | −20 | −16 | −16 | −10 | −8 | −10 | −36 |
| O(II) | Ti(I) | 100 | 132 | 124 | 128 | 120 | 118 | 150 |
| | O(II) | 4 | 2 | 2 | 2 | 2 | 2 | 2 |
| | Sr(II) | −8 | −8 | −10 | −4 | −4 | −6 | −20 |
| | Ti(III) | 78 | 92 | 92 | 84 | 86 | 88 | 104 |
| | O(III) | −38 | −30 | −32 | −24 | −24 | −26 | −42 |
| O(III) | Sr(II) | −4 | −4 | −6 | 0 | −2 | −2 | −18 |
| | O(III) | −42 | −34 | −36 | −30 | −30 | −32 | −44 |
| | Ti(III) | 62 | 86 | 86 | 76 | 78 | 74 | 114 |
| | Sr(IV) | −8 | −8 | −10 | −4 | −4 | −6 | −22 |
| | O(IV) | −46 | −36 | −34 | −30 | −18 | −20 | −44 |
| O(IV) | Ti(III) | 54 | 78 | 80 | 68 | 72 | 70 | 106 |
| | O(IV) | 4 | 2 | 2 | 2 | 2 | 2 | 2 |
| | Sr(IV) | −10 | −8 | −10 | −4 | −30 | −6 | −22 |

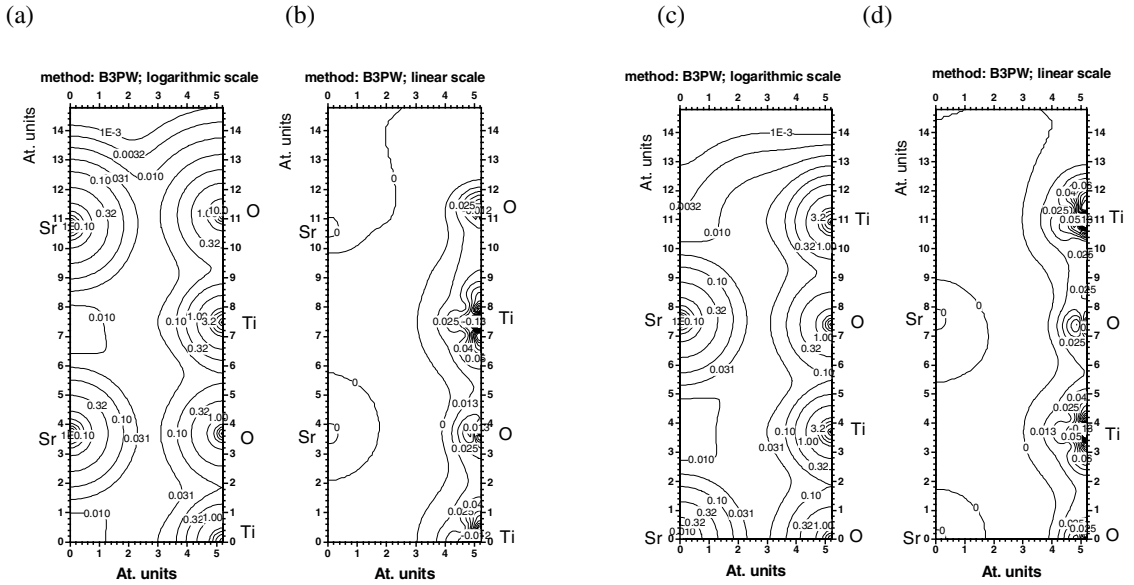


**Fig. 1** Total (parts a and c) and difference (parts b and d) electron density maps in the cross section perpendicular to the (100) surface with SrO (parts a, b) and $TiO_2$ (parts c, d) terminations.

*Bond populations* between atoms for the $TiO_2$ termination are given in Table 6. Let us, for the analysis, look at the particular B3PW results. The major effect observed here is strengthening of the Ti–O chemical bond near the surface, which is already pronounced in the bulk (Table 2), where the Ti–O bond is considerably populated (82 m*e*). The Ti–O bond population for the $TiO_2$-terminated surface is 128 m*e*, which is about 50% larger than the relevant values in the bulk. The Ti–O populations in the direction perpendicular to the surface, i.e. between Ti and O atoms in the first and second, the second and third plane, and lastly, the third and fourth planes (124 m*e*, 92 m*e*, and 86 m*e*) also exceed the bulk value. In contrast, the Sr–O populations are very small and even negative which indicates the repulsion. (The same is true for O–O interactions). This effect is also well seen from Sr effective charges, which are close to the formal ionic charge of +2*e*. Calculated total electron densities confirm the Ti–O covalency effects discussed above, whereas the difference electron density maps (Fig. 1) calculated with respect to the superposition density for $Sr^{2+}$, $Ti^{4+}$, and $O^{2-}$ ions, demonstrate considerable *charge density redistribution* for both $SrTiO_3$ surface terminations. These maps show that there is no trace of covalent bonding between Sr and O atoms. The Sr atoms nearest the surface are polarized. Their electronic density is shifted inwards the bulk in the case of the $TiO_2$-terminated surface and outwards on the SrO-terminated surface. For both terminations the nearest the surface Ti–O bond becomes stronger, but the next nearest bond becomes weaker.

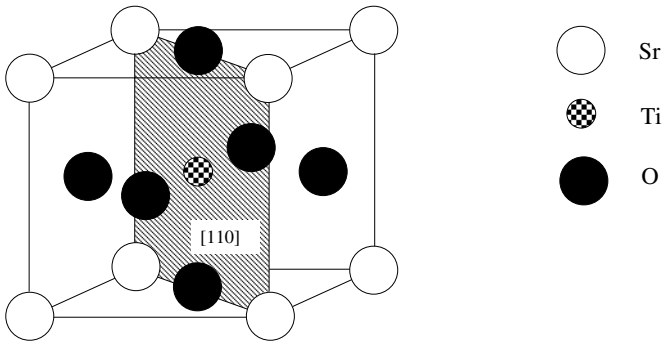


**Fig. 2** Sketch of the cubic $SrTiO_3$ perovskite structure with shaded (110) surfaces.

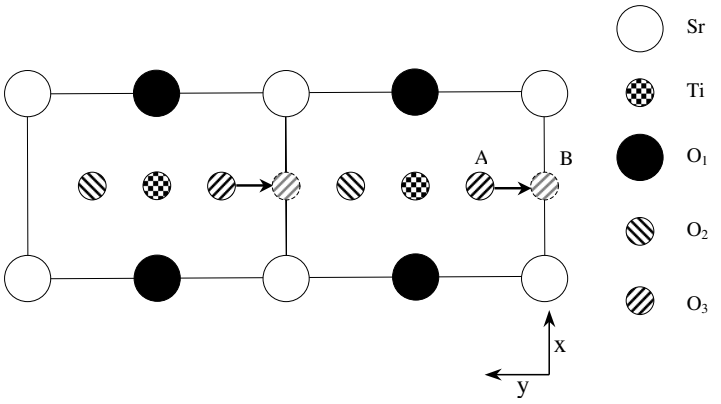


**Fig. 3** Top view of the (110) O-terminated surface, directions of the O atom displacement are shown by arrows. In our model, we remove atoms $O_2$ from the O-terminated surface and search for the atomic relaxations when $O_3$ are placed initially into asymmetric or symmetric positions, A and B, respectively. Atoms of Ti, Sr and $O_1$ lie in the second plane below the O-surface plane.

**4. The (110) surface** The well-known problem with modelling the (110) surfaces of $SrTiO_3$ (Fig. 2) is that they consist of charged planes. In other words, if the (110) surface were to be modelled exactly as one would expect after ideal crystal cleavage, it would have an infinite dipole moment perpendicular to the surface, which would make the surface unstable. To avoid this problem, in our calculations, we removed half the O atoms from the O-terminated surface (Fig. 2 and Fig. 3). As a result, we obtained the so-called type-II stable surface (Fig. 3) with charged planes, but a zero dipole moment [61]. The relevant surface cells are built from neutral five-atom elements from three successive planes, which are shown as encircled dashed ellipses in Figs. 4 and 5.

The initial atomic configuration A for the O-terminated surface, where every second surface O atom is removed and others occupy the same sites as in the bulk structure, is called hereafter *asymmetric*. In the alternative initial configuration B which we call *symmetric*, O atoms are placed in the middle of the distance between equivalent O atoms in the bulk (Fig. 5). For the asymmetric configuration, all first and second layer surface atoms during geometry optimization are displaced along both the *z*-axis perpendicular to the surface and on-plane, i.e. in the direction parallel to the surface, whereas in the symmetric configuration they are displaced by symmetry only perpendicularly to the surface. Earlier these two configurations were modelled by means of the classical SM [19]. A comparison of our HF calculations for the configuration A with these SM simulations presented in Table 7 demonstrates their qualitative agreement.

**5. Quantum chemical modelling of electron polarons** In our calculations of the electron polarons in $BaTiO_3$ we relaxed 6 O atoms around the central Ti atom, where the electron polaron is mainly localized,

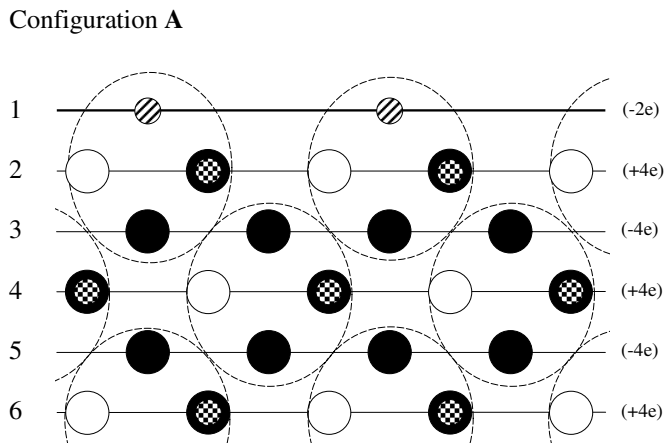


**Fig. 4** Side view of the possible initial configuration A.

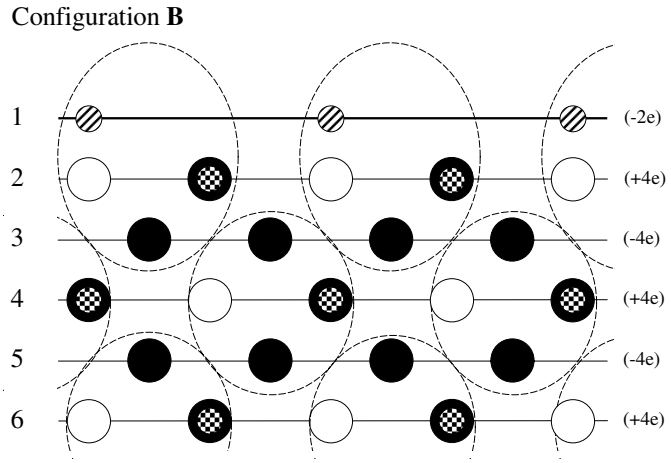


**Fig. 5** Side view of the possible initial configuration B.

**Table 7** Atomic relaxation of the uppermost two layers in the O-terminated $SrTiO_3$ (110) surfaces for the case of asymmetric, A-type termination. $\Delta y$ and $\Delta z$ are on-plane and perpendicular to the surface atomic displacements (in per cent of bulk lattice constant).

| layer | atom | $\Delta y$, *ab initio* | $\Delta y$, SM [19] | $\Delta z$, *ab initio* | $\Delta z$, SM [19] |
|---|---|---|---|---|---|
| 1 | O | −10.53 | −8.54 | −10.41 | −14.2 |
| 2 | Ti | −7.71 | −8.27 | −1.36 | −2.37 |
| 2 | Sr | −7.30 | −10.79 | 2.2 | 4.10 |
| 2 | O | 6.15 | 8.20 | 6.65 | 5.71 |

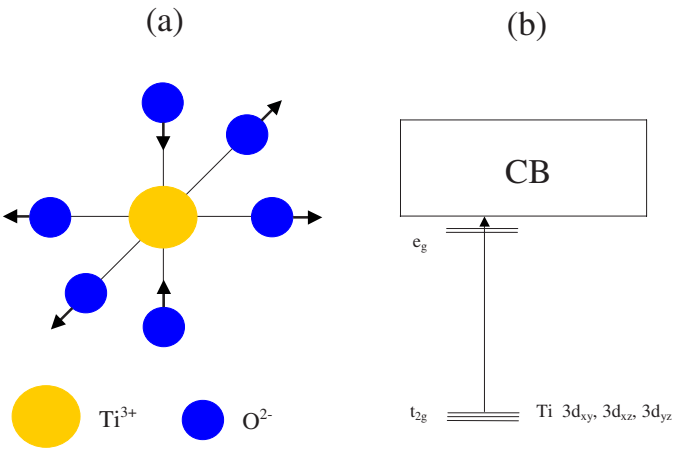


**Fig. 6** (online colour at: www.interscience.wiley.com) a) Asymmetric oxygen relaxation around the central Ti atom where the self-trapped electron in $BaTiO_3$ is localized. Two O atoms move towards a central Ti atom along the *z*-axis and the other four O atoms relax outwards in the *x*–*y* plane. b) Positions of 3*d* states of a central Ti atom in the $BaTiO_3$ band gap.

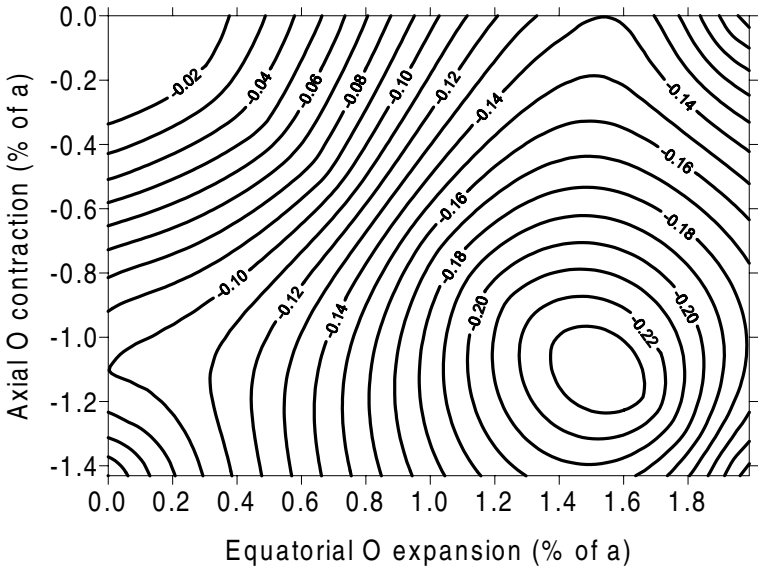


**Fig. 7** A contour plot of the lattice energy gain due to outward $x-y$ displacement of four equatorial O atoms and the inward relaxation of two oxygens along the $z$-axis.

and kept fixed all other atoms, see Fig. 6. (We restricted ourselves to the cubic $BaTiO_3$ phase.) As a result of geometry optimization, we found that the energy minimum of the system corresponds to outward displacement of four nearest equatorial O atoms by 1.53% $a_0$ (lattice constant) and relaxation of the remaining two nearest O atoms inwards, by 1.1% $a_0$ along the $z$ axis. The total energy gain of a system due to lattice relaxation around Ti atom is 0.24 eV, see Fig. 7.

As a result of combined breathing mode and the Jahn-Teller (JT) effect, initially three-fould degenerate ground state of the system with symmetry $t_{2g}$ splits into two levels, nondegenerate and twofold degenerate. As a result of asymmetric geometry relaxation a considerable electron density is localized on the Ti $3d_{xy}$, $3d_{xz}$ and $3d_{yz}$ atomic orbitals. In fact, about 80 percent of an extra electron density is localized on Ti atom, which confirms a model of small-radius electron polaron in $BaTiO_3$. Another two empty levels with $e_g$ symmetry are located close to CB bottom. The calculated $t_{2g}$ ground state symmetry agrees well with the experimentally detected [62]. We have calculated also the electron polaron optical absorption energy, using the ΔSCF scheme, and found it to be 0.69 eV. The absorption process corresponds to a charge transfer to the nearest Ti atom. This absorption band has been detected recently experimentally using picosecond laser excitation [63], with absorption energy ≈0.6 eV. Our calculated electron polaron energy for $BaTiO_3$ (0.69 eV) is also close to the $Nb^{4+}$ polaron absorption band detected recently around 0.72 eV in strontium barium niobate [64]. This lies also in the same energy range as our previous electron polaron calculations in $ABO_3$ [28].

**6. Calculations of triplet excitons in $ABO_3$ perovskites** In our previous study [28, 65] we modelled the triplet exciton in a cubic phase of $KNbO_3$ and $KTaO_3$ perovskites. Our main conclusion is that the triplet exciton consists mainly of three atoms: two Nb atoms ($Nb_1$ and $Nb_2$) and one $O_1$ atom between them (in the $KNbO_3$ case). The main effect is a charge transfer (≈0.5$e$) from the $O_1$ atom to the nearest $Nb_1$ atom. This increases the vibronic interaction and induces a local lattice instability. This results in a formation of the excited state with a new equilibrium charge transfer and lattice relaxation [31, 32]. As a result of modelling, we found that the CTVE consists of a pair of spatially well correlated electron and hole polarons localised mainly on the nearest $Nb_1$ and $O_1$ atoms. These two atoms are displaced from the lattice sites towards each other due to the effective Coulomb attraction. This is accompanied with a strong (a few eV) vibronic energy reduction. These properties are in agreement with the semiphenomenological CTVE-model proposed earlier [66, 67].

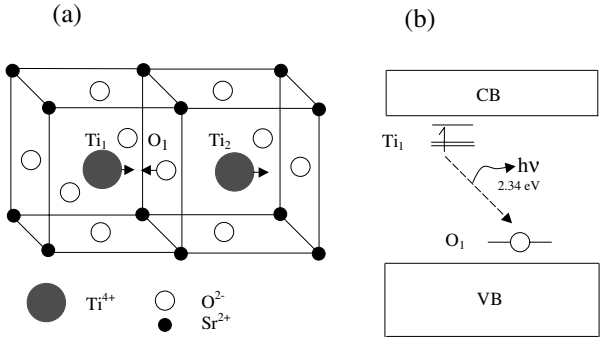


**Fig. 8** a) INDO-calculated triad atomic structure of a single CTVE in $SrTiO_3$. The directions of displacement of three active $Ti_1$–$O_1$–$Ti_2$ ions constituting the triad centre are shown. b) Schematic view of the Ti and O energy levels induced by the CTVE in the band gap and its luminescence.

These findings are confirmed by our present calculations for the exciton in a cubic phase of $SrTiO_3$. The oxygen ion $O_1$ in $SrTiO_3$ is displaced by 4.6% $a_0$ (lattice constant) towards the $Ti_1$ ion. Simultaneously, this $Ti_1$ ion reveals a displacement of 2.6% $a_0$ towards the $O_1$ ion, whereas another $Ti_2$ ion (which is located on the other side from the oxygen ion $O_1$ along the CTVE-axis) shows a repulsion from the $O_1$ and is displaced outwards by 4.1% $a_0$, see Fig. 8. We obtained that the total energy reduction in CTVE in $SrTiO_3$ due to the lattice relaxation of $O_1$, $Ti_1$ and $Ti_2$ is quite appreciable, –2.04 eV. The most significant charge transfer (0.45$e$) occurs between $O_1$ and $Ti_1$ ions. Results of the INDO calculations for the lattice energy gain $E_{rel}$ and displacements of three basic atoms involved in the exciton formation for four $ABO_3$ perovskites are collected in Table 8.

The strong lattice distortion caused by the CTVE induces local energy level in the $SrTiO_3$ band gap. Namely, the $O_1$ energy level with the hole is located 0.7 eV above the VB top, its wave function consist mainly of its $2p_x$ atomic orbitals directed towards the $Ti_1$ atom. On the other hand, two closely located $Ti_1$ energy levels (one of them is two-fold degenerate) appear at 0.6 eV below the CB. They have $t_{2g}$ symmetry and consist mainly of $3d_{xy}$ atomic orbitals of $Ti_1$ with admixture of $Ti_2$ ion atomic orbitals. Table 8 presents the distance of the donor and acceptor one-electron energy levels from the relevant bands for all four perovskites.

In our model the luminescence arises due to the electron transfer from the donor level (close to the CB bottom and formed by the electron polaron) to the hole level (close to the VB created by the hole polaron). As one can see in Table 9, the luminescence energies calculated using the ΔSCF method are close to the experimentally observed values for all four $ABO_3$ crystals. The luminescence quenching energy calculated for $KNbO_3$ as a typical $ABO_3$ crystal, is very small, <0.1 eV, which explains why the green luminescence is observed only at very low temperatures.

**7. Conclusions** A comparison of ab initio HF and DFT calculations employing different exchange-correlation functionals and localized/plane wave basis sets clearly demonstrates their good agreement for the rumpling and the relative displacements of the second and third planes nearby the $SrTiO_3$ surface.

**Table 8** Results of charge transfer vibronic exciton calculations for cubic phases of four $ABO_3$ perovskites performed by means of the INDO method. $E_{rel}$ is the lattice energy gain, $\Delta$ is $B_1$, $O_1$, $B_2$ atomic displacement (Fig. 8a) along the (100) axis (in per cent of lattice constant), $\varepsilon_d$, $\varepsilon_a$ are distances from donor (acceptor) levels to the edges of relevant bands.

| crystal | $E_{rel}$ (eV) | $\Delta$ (% of $a_0$) | $\varepsilon_d$ (eV) | $\varepsilon_a$ (eV) |
|---|---|---|---|---|
| $SrTiO_3$ | 2.04 | 2.6; –4.6; 4.1 | 0.6 | 0.7 |
| $BaTiO_3$ | 2.20 | 2.8; –4.7; 4.2 | 0.65 | 0.8 |
| $KNbO_3$ | 2.37 | 2.9; –4.9; 4.3 | 0.7 | 0.9 |
| $KTaO_3$ | 2.71 | 3.1; –5.2; 4.5 | 0.8 | 1.0 |

**Table 9** Green luminescence energies in $ABO_3$ perovskites (in eV) as calculated by means of INDO and detected experimentally.

| crystal | calculated | experimental |
|---|---|---|
| $SrTiO_3$ | 2.34 | 2.4 |
| $BaTiO_3$ | 2.30 | 2.5 |
| $KNbO_3$ (cubic phase) | 2.17 [28] | 2.15 |
| $KNbO_3$ (orthorhombic phase) | 2.2 | 2.15 |
| $KTaO_3$ | 2.14[28] | 2.2–2.3 |

Further comparison of ab initio calculations corresponding to 0 K with experiments performed at room temperature needs a detailed analysis of anharmonic vibrations of the surface atom (in particular Ti). On the other hand, several diffraction experiments used so far clearly contradict each other. This could arise due to both difference in sample preparations and as a result of the different interpretations of indirect experiments.

Our *ab initio* calculations indicate a considerable increase of Ti–O bond covalency near the surfaace. This could have impact on the electronic structure of surface defects (e.g., *F* centers), as well as affect the adsorption and surface diffusion of atoms and small molecules relevant in catalysis.

Our quantum chemical INDO calculations gave additional evidence for the existence of electron polarons in $BaTiO_3$ crystals which are expected to be stable at low temperatures. The calculated $t_{2g}$ ground-state symmetry for the electron polaron is in agreement with experimental observations [62]. The theoretically calculated electron polaron absorption energy in $BaTiO_3$ (0.69 eV) agrees well with the only experimental estimate of 0.6 eV [63].

Our calculations for a series of perovskite materials – $SrTiO_3$, $BaTiO_3$, $KNbO_3$ and $KTaO_3$ – give a strong support to the "green" luminescence in these crystals as a result of the recombination of electrons and holes forming the charge transfer vibronic exciton rather than due to the electron transitions in a $MeO_6$ complex. Our results also demonstrate that well-parametrised quantum chemical methods are a very efficient tool for the study of optical properties of advanced perovskite materials.

**Acknowledgements** This study is supported in part by DFG, NATO (grant PST.CLG. 977561) and European Center of Excellence in Advanced Materials Research and Technology in Riga, Latvia.

## References

[1] M. E. Lines and A. M. Glass, Principles and Applications of Ferroelectrics and Related Materials (Clarendon, Oxford, 1977).
[2] C. Noguera, Physics and Chemistry at Oxide Surfaces (Cambridge Univ. Press, N.Y., 1996).
[3] J. F. Scott, Ferroelectric Memories (Springer, Berlin, 2000).
[4] Proceedings of the Williamsburg workshop on Fundamental Physics of Ferroelectrics-99, J. Phys. Chem. Sol. **61**, No. 2 (2000).
[5] N. Bickel, G. Schmidt, K. Heinz, and K. Müller, Phys. Rev. Lett. **62**, 2009 (1989).
[6] T. Hikita, T. Hanada, M. Kudo, and M. Kawai, Surf. Sci. **287/288**, 377 (1993).
[7] M. Kudo, T. Hikita, T. Hanada, R. Sekine, and M. Kawai, Surf. Interface Anal. **22**, 412 (1994).
[8] Y. Kido, T. Nishimura, Y. Hoshido, and H. Mamba, Nucl. Instrum. Methods B **161–163** 371 (2000).
[9] G. Charlton, S. Brennan, C. A. Muryn, R. McGrath et. al., Surf. Sci. **457**, L376 (2000).
[10] J. Padilla and D. Vanderbilt, Surf. Sci. **418**, 64 (1998).
[11] J. Padilla and D. Vanderbilt, Phys. Rev. B **56**, 1625 (1997).
[12] B. Meyer, J. Padilla, and D. Vanderbilt, Faraday Discussions **114**, 395 (1999).
[13] F. Cora and C. R. A. Catlow, Faraday Discussions **114**, 421 (1999).
[14] R. E. Cohen, Ferroelectrics **194**, 323 (1997).
[15] L. Fu, E. Yashenko, L. Resca, and R. Resta, Phys. Rev. B **60**, 2697 (1999).
[16] C. Cheng, K. Kunc, and M. H. Lee, Phys. Rev. B **62**, 10409 (2000).
[17] A. A. Demkov, phys. stat. sol. (b) **226**, 57 (2001).

[18] S. Tinte and M. G. Stachiotti, AIP Conf. Proc. **535** (ed. R. Cohen) 273 (2000).
[19] E. Heifets, E. A. Kotomin, and J. Maier, Surf. Sci. **462**, 19 (2000).
[20] E. A. Kotomin, R. I. Eglitis, J. Maier, and E. Heifets, Thin Solid Films **400**, 76 (2001).
[21] L. Shiv, J. L. Sorensen, E. S. Polzik, and G. Mizel, Opt. Lett. **20**, 2270 (1995).
[22] E. R. Hodgson, C. Zaldo, and F. Agullo-Lopez, Solid State Commun. **75**, 351 (1990).
[23] L. Grigorjeva, D. Millers, E. A. Kotomin, and E. S. Polzik, Solid State Commun. **104**, 327 (1997).
[24] L. Grigorjeva, D. K. Millers, V. Pankratov, R. T. Williams, R. I. Eglitis, E. A. Kotomin, and G. Borstel, Phys. Rev. B, 2003, submitted.
[25] E. A. Kotomin, N. E. Christensen, R. I. Eglitis, and G. Borstel, Comput. Mater. Sci. **10**, 339 (1998).
[26] E. A. Kotomin, R. I. Eglitis, and G. Borstel, Comput. Mater. Sci. **17**, 290 (2000).
[27] T. Hasegawa, M. Shirai, and K. Tanaka, J. Lumin. **87–89**, 1217 (2000).
[28] E. A. Kotomin, R. I. Eglitis, and G. Borstel, J. Phys.: Condens. Matter **12**, L557 (2000).
[29] G. Koshek and E. Kubalek, phys. stat. sol. (a) **79**, 131 (1983).
[30] V. Vikhnin and S. E. Kapphan, Phys. Solid. State **40**, 834 (1998).
[31] V. S. Vikhnin, R. I. Eglitis, S. E. Kapphan, E. A. Kotomin, and G. Borstel, Europhys. Lett. **56**, 702 (2001).
[32] V. S. Vikhnin, R. I. Eglitis, S. E. Kapphan, G. Borstel, and E. A. Kotomin, Phys. Rev. B **65**, 104304 (2002).
[33] C. Blasse, Mater. Res. Bull. **18**, 525 (1983).
[34] M. Causa and A. Zupan, Chem. Phys. Lett. **220**, 145 (1994).
[35] V. R. Saunders, R. Dovesi, C. Roetti, M. Causa, N. M. Harrison, R. Orlando, and C. M. Zicovich-Wilson, Crystal-98 User Manual (University of Turin, 1999).
[36] E. Heifets, R. I. Eglitis, E. A. Kotomin, J. Maier, and G. Borstel, Phys. Rev. B **64**, 235417 (2001).
[37] R. E. Cohen, Nature **358**, 136 (1992).
[38] R. E. Cohen and H. Krakauer, Phys. Rev. B **42**, 6416 (1990).
[39] K. M. Rabe and U. W. Waghmare, J. Phys. Chem. Solids **57**, 1397 (1996).
[40] K. M. Rabe and U. W. Waghmare, Phys. Rev. B **52**, 13236 (1995).
[41] J. A. Pople and D. L. Beveridge, Approximate Molecular Orbital Theory (McGraw-Hill, New York, 1970).
[42] A. L. Shluger, Theor. Chim. Acta **66**, 355 (1985).
[43] E. Stefanovich, E. Shidlovskaya, A. L. Shluger, and M. Zakharov, phys. stat. sol. (b) **160**, 529 (1990).
[44] R. I. Eglitis, S. V. Izvekov, and M. R. Philpott, Comput. Mater. Sci. **17**, 275 (2000).
[45] R. I. Eglitis and M. R. Philpott, Chin. Phys. Lett. **19**, 389 (2002).
[46] J. T. Devreese, V. M. Fomin, E. P. Pokatilov, E. A. Kotomin, R. I. Eglitis, and Yu. F. Zhukovskii, Phys. Rev. B **63**, 184304 (2001).
[47] R. I. Eglitis, M. M. Kuklja, E. A. Kotomin, A. Stashans, and A. I. Popov, Comput. Mater. Sci. **5**, 298 (1996).
[48] E. A. Kotomin, M. M. Kuklja, R. I. Eglitis, and A. I. Popov, Mater. Sci. Eng. B **37**, 212 (1996).
[49] R. I. Eglitis, E. A. Kotomin, and G. Borstel, phys. stat. sol. (b) **208**, 15 (1998).
[50] R. I. Eglitis, A. V. Postnikov, and G. Borstel, phys. stat. sol. (b) **209**, 187 (1998).
[51] A. Stashans and M. Kitamura, Solid State Commun. **99**, 583 (1996).
[52] R. I. Eglitis, A. V. Postnikov, and G. Borstel, Phys. Rev. B **54**, 2421 (1996).
[53] R. I. Eglitis, A. V. Postnikov, and G. Borstel, Phys. Rev. B **55**, 12976 (1997).
[54] R. I. Eglitis, E. A. Kotomin, and G. Borstel, J. Phys.: Condens. Matter **12**, L431 (2000).
[55] R. I. Eglitis, E. A. Kotomin, G. Borstel, and S. Dorfman, J. Phys.: Condens. Matter **10**, 6271 (1998).
[56] R. I. Eglitis, N. E. Christensen, E. A. Kotomin, A. V. Postnikov, and G. Borstel, Phys. Rev. B **56**, 8599 (1997).
[57] E. A. Kotomin, R. I. Eglitis, A. V. Postnikov, G. Borstel, and N. E. Christensen, Phys. Rev. B **60**, 1 (1999).
[58] R. I. Eglitis, E. A. Kotomin, A. V. Postnikov, N. E. Christensen, M. A. Korotin, and G. Borstel, Ferroelectrics **229**, 69 (1999).
[59] H. Pinto and A. Stashans, Comput. Mater. Sci. **17**, 73 (2000).
[60] A. Stashans, Mater. Chem. Phys. **68**, 126 (2001).
[61] P. W. Tasker, J. Phys. C **20**, 4383 (1987).
[62] S. Köhne, O. F. Schirmer, H. Hesse, T. W. Kool, and V. S. Vikhnin, J. Supercond. **12**, 193 (1999).
[63] H.-J. Reyher, private communication, 2001.
[64] M. Gao, S. Kapphan, R. Pankrath, and J. Zhao, phys. stat. sol. (b) **217**, 999 (2000).
[65] V. S. Vikhnin, H. Liu, W. Jia, S. Kapphan, R. I. Eglitis, and D. Usvyat, J. Lumin. **83/84**, 109 (1999).
[66] V. S. Vikhnin, Ferroelectrics **199**, 25 (1997).
[67] V. S. Vikhnin, Ferroelectrics Lett. **25**, 27 (1999).